

Theoretical Study of Electronic Structures of [Peroxoporphinato]manganate $[Mn(P)(O_2)]^-$ Anion

Yasunori Yoshioka,* Hideaki Sano, and Masaki Mitani

Chemistry Department, Graduate School of Engineering, Mie University, 1577 Kurimamachiya, Tsu 514-8507

Received November 15, 2005; E-mail: yyoshi@chem.mie-u.ac.jp

Geometries and electronic structures of the quintet and septet states of the $[Mn(P)(O_2)]^-$ (P: porphinato) anion were theoretically investigated. Four local minimum geometries with two side-on additions of O_2 to MnP, **1** ($^5B_2$) and **3** ($^7A_2$), and two end-on additions of O_2, **2** ($^5A''$) and **4** ($^5A'$), were found. One of the side-on forms, **1**, corresponds to that observed by X-ray crystallographic study. **3** is a septet state with higher spin than the quintet states of **1**, **2**, and **4**. Each of the two end-on forms has the corresponding transition state with the side-on geometry. Energy differences among **1**, **2**, and **3** are less than 1 kcal mol^{-1}. The electronic structures of four local minimum states were essentially different. **1** has an electronic structure presented as $[Mn^{III}(O_2^{2-})]^-$. **2** has antiferromagnetically coupled diradical character presented by the formal chemical formula of $[Mn^{II\bullet}(O_2^{\bullet-})]^-$. **3** has ferromagnetically coupled diradical character. **4** is presented by $[Mn^{II}(O_2^-)]^-$.

It has been well recognized that manganese interacts with dioxygen and its reduced derivatives in biological systems in numerous ways. The nuclearity of Mn sites that interact with dioxygen in biology ranges from mononuclear (MnSOD; manganese superoxide dismutase) and dinuclear (MnRR; manganese ribonucleotide reductase) to tetranuclear (OEC; oxygen-evolving complex in photosystem II), making use of the Mn(II), Mn(III), and Mn(IV) oxidation states.[1–5] In an early stage of study on manganese chemistry, much of the work involved the oxygenation of Mn–porphyrin complexes, even the Mn sites in MnSOD and OEC were non-heme sites.[6]

The $[Mn(TPP)(O_2)]$ (TPP: tetraphenylporphinato) complex, which was prepared as the first dioxygen adduct for the Mn–porphyrin complex by Basolo and co-workers using synthetic manganese porphyrin,[7] was formed by the replacement of pyridine in $[Mn^{II}(TPP)(py)]$. The EPR observation of this complex exhibited an $S = 3/2$ ground state that indicates a Mn(IV) formal oxidation state with a large transfer of electron density from manganese to O_2 and an absence of spin density on O_2 upon binding.[7] Thus, this complex could be formally denoted as $[Mn^{IV}(TPP)(O_2^{2-})]$.

The $[Mn^{III}(TPP)(O_2)]^-$ anion has been prepared as potassium cryptate $[K(K222)]^+$ salts of the [peroxotetraphenylporphinato]manganate(III) anion by Valentine and co-workers,[8] and its structure was first characterized by X-ray crystallographic study. The dioxygen is bound to manganese in a side-on form, and manganese lies 0.764 Å above the least-squares plane based on four pyrrole nitrogens of porphyrin toward the peroxo ligand. $[Mn^{III}(TPP)(O_2)]^-$ was originally prepared by Valentine and Quinn[9] and was believed to be $[Mn^{II}(TPP)(O_2^-)]^-$ because of its lack of the split Soret band. However, Valentine and co-workers[8] concluded from the X-ray crystallographic observation that the oxidation state of Mn is Mn(III) denoted as $[Mn^{III}(TPP)(O_2^{2-})]^-$ rather than Mn(II); even additional support[10] for Mn(II) was provided from a deuterium NMR study by Shirazi and Goff. Valentine et al. also estimated the electronic structures from iterative extended Hückel (IEH) and INDO/s of semiempirical molecular orbital methods and showed that the ground state of the d^4 complex is $(d_{xy} - O_2\pi_{gy})^1(d_{yz})^1(d_{z^2})^1(d_{x^2-y^2})^1$ in the coordinate system of the *xy*-plane defined by the pyrrole nitrogens and the *x*-axis parallel to the O–O axis.[8,11] Shirazi and Goff predicted that the Mn(II) center with a singly occupied $d_{x^2-y^2}$ orbital would have strong antiferromagnetic coupling to the unpaired spin on a superoxo ligand.[10] Thus, it looks unclear whether the oxidation state of manganese in $[Mn(TPP)(O_2)]^-$ is Mn(II) or Mn(III). The purpose of this work is to give the oxidation state of Mn by performing theoretical calculations of possible geometries and electronic structures of $[Mn(P)(O_2)]^-$ (P: porphinato).

The Mn–porphyrin complex and its derivatives have attracted interest as versatile oxidation catalysts of alkanes and alkenes.[12–20] Their typical Mn–porphyrins complexes are [Mn(P)Cl], [Mn(P)O], and $[Mn(P)O]^+$. Zwaans and co-workers have performed ab initio calculations on $[Mn^{III}(P)Cl]$ and its cation and anion.[12,13] The ground state of a neutral $[Mn^{III}(P)Cl]$ is a quintet state of the highest spin state with the electron configuration of $(d_{z^2})^1(d_{xy})^1(d_{yz})^1(d_{xz})^1$ with the transfer of electron densities from Mn to Cl. The ground state of the anion $[Mn^{II}(P)Cl]^-$ is a sextet state with the electron configuration of $(d_{z^2})^1(d_{x^2-y^2})^1(d_{xy})^1(d_{yz})^1(d_{xz})^1$, in good agreement with the result of the IEH calculation shown by Valentine and co-workers.[8] An added electron occupied the unoccupied 3d orbital of Mn with spin parallel to others, and Cl is a Cl anion with a fully occupied electron configuration of $(3s)^2(3p)^6$. Then, the oxidation state of Mn changes from Mn(III) to Mn(II). In the case of [Mn(P)O], and $[Mn(P)O]^+$, the oxidation states of Mn in the neutral and positively charged systems are Mn(IV) and Mn(V), respectively, with a large transfer of electron density from the 3d orbital of Mn to the doubly degenerate and singly occupied p-orbitals of the O atom. [Mn(P)Cl] and [Mn(P)O] have similar electron configurations where the ligands are fully occupied such as $(s)^2(p)^6$.

Published on the web August 7, 2006; doi:10.1246/bcsj.79.1201

$[Mn(P)(O_2)]^-$ is different from [Mn(P)Cl] and [Mn(P)O], since the unoccupied orbitals π_y^* and π_z^* of O_2 interact with 3d-orbitals of Mn in a different manner. Therefore, $[Mn(P)(O_2)]^-$ is a more interesting and more complex system than them.

In this work, we focus on the oxidation state of Mn, and the geometries and electronic structures of the $[Mn(P)(O_2)]^-$ system. The possible electron and spin configurations of $[Mn(P)(O_2)]^-$ were investigated using high quality calculations at the unrestricted B3LYP level. Four stable geometries were found. Two of the four are side-on forms and the others are end-on forms. It is shown that the electronic structures of these four states are different in the interaction between Mn and O_2. In addition, two side-on forms corresponding to the transition states for two end-on forms were also found.

Calculation Details

Obtaining the Electronic Structures. Since correlation effects are important to elucidate the transition-metal systems, the usual Hartree–Fock methods lead to poor estimations for the complex systems of manganese, porphyrin, and O_2 molecule. The hybrid exchange-correlation functional B3LYP method[21–24] was most widely used for the transition-metal system, and provided results in good agreement with experiments for mononuclear systems. In order to confirm the applicability of the B3LYP method for the manganese mononuclear system, we estimated the dissociation energy of $[MnCH_2]^+$ as a test calculation. For the $[MnCH_2]^+$ system, the UHF method gives the dissociation energy of 44.3 kcal mol^{-1} with a MINI basis set,[25,26] The UMP4 method gives 66.4 kcal mol^{-1},[26] and the SDCI method gives 36.0 kcal mol^{-1} with an augmented Wachters basis set[27] for Mn and TZP basis set for C and H.[28] All these results largely deviate from the experimental value of 96 ± 4 kcal mol^{-1}.[29] However, using the B3LYP method with the LanL2DZ basis set[30] for Mn and 6-31G* basis set[31] for C and H, the dissociation energy was estimated to be 84.8 kcal mol^{-1}, which is in reasonable agreement with the experimental value. In this work, we employed the B3LYP method to estimate the electronic structures of $[Mn(P)(O_2)]^-$. The LanL2DZ basis set was employed for the Mn atom and the 6-31G* basis set for porphyrin. The 6-311+G* basis set,[32] which can feasibly accept extra electrons, was used for dioxygen. All calculations were carried out using the program package Gaussian 98.[33]

It is well recognized that it is a difficult task to investigate the electronic structures of the transition-metal systems due to the degeneracy of d-orbitals that cause lots of possible electron spin configurations and spin states in narrow energy regions. In some cases, metal interacts with a ligand in a manner of ferromagnetic and antiferromagnetic spin couplings, in addition to the usual bond formation and coordinate bond. Thus, we have to search all wavefunctions corresponding to possible electron and spin configurations. For calculations at the SCF level, we have to make the appropriate initial guess corresponding to the desired state.

Before we examine the geometries and electronic structures of $[Mn(P)(O_2)]^-$, we like to consider simply the electron spin configurations of $[Mn(O_2)]^-$ in $[Mn(P)(O_2)]^-$. Suppose that $[Mn(O_2)]^-$ is formally presented by $[Mn^{III}(O_2^-)]$ plus an extra electron, as shown in Fig. 1 schematically for interaction in $[Mn^{III}(O_2^-)]$, Mn(III) has $(3d)^4$ electron spin configuration, and O_2^- has a doubly occupied π^* orbital and a singly occupied π^* orbital. It is schematically shown by (a) in Fig. 1. In this simple diagram, bond formations by orbital interactions between Mn(III) and O_2^- are not involved for the simplicity even though the bonds exist. They are dependent on the geometric configurations of Mn(P) and O_2. The addition of an extra electron to yield $[Mn^{III}(O_2)]^-$ causes three possible electron spin configurations such as (b), (c), and (d) shown in Fig. 1. For **S1** in (b), an extra electron is put into a singly occupied π^* orbital of O_2^- to give O_2^{2-} with fully occupied π^* orbitals. The spin multiplicity for this configuration is given by 5, which is a quintet state, and the total charge is -1. In this spin configuration **S1**, $[Mn^{III}(O_2)]^-$ is formally presented by $[Mn^{III}(O_2^{2-})]^-$, which is expected to correspond to $[Mn^{III}(TPP)(O_2^{2-})]^-$, as proposed by Valentine and coworkers.[8,11] For (c), an extra electron is added into the unoccupied 3d orbital of Mn. The spins of the added 3d orbital and the singly occupied π^* orbital cause three possible interactions. **S2** presents covalent bond formation between their orbitals with transfer of electron density from Mn to O_2. This is denoted as $[Mn^{III}(O_2^{2-})]^-$, which is indistinguishable from **S1**. **S3** is an antiferromagnetic spin-coupling diradical, and **S4** is a ferromagnetic spin-coupling diradical. Their formal presentations for $[Mn^{III}(O_2)]^-$ are $[Mn^{II\bullet}(O_2^{\bullet-})]^-$, which is expected to cor-

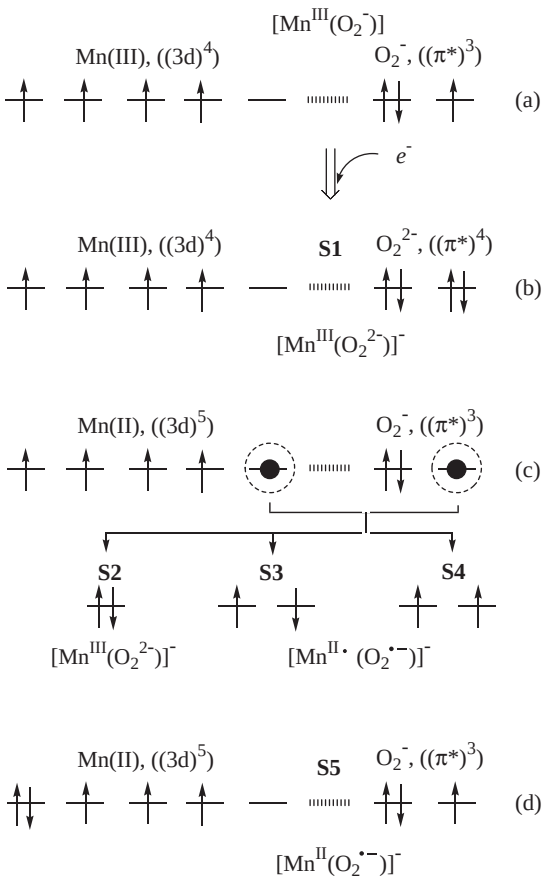

Fig. 1. Schematic diagrams of possible electron spin configurations in $[Mn(P)(O_2)]^-$, supposing that they are constructed from $[Mn^{III}(O_2^-)]$ plus an extra electron.

respond to the original $[Mn^{II}(TPP)(O_2^-)]^-$ proposed by Goff and co-worker.[9,10] In these cases, the oxidation state of Mn is Mn(II) with the $(3d)^5$ configuration rather than Mn(III) with the $(3d)^4$ configuration of **S1**. The spin multiplicities of systems are given by 5 for **S2** and **S3**, and 7 for **S4**. For **S5** in (d), an extra electron is put into a singly occupied 3d orbital of Mn to make a doubly occupied orbital with paired up- and down-spins. The spin multiplicity is also given by 5, since O_2^- is not altered from a singly occupied π^* orbital. These four different spin configurations, **S1**, **S2**, **S3**, and **S5**, have the same spin multiplicity of 5 and the **S4** spin configuration has 7.

The calculations to obtain the optimized states with all possible electron spin configurations shown in Fig. 1 were carried out as follows. For all spin configurations, the geometries of the systems were held with the side-on form, since orbitals are distinguishable because of the higher symmetry than the end-on form. First of all, the geometry of Mn–porphyrin $[Mn^{II}(P)]$ with the total charge of 0 and the spin multiplicity of 6 was optimized. Using the optimized geometry of $[Mn^{II}(P)]$, dioxygen was added to give the side-on form with the distances of 1.91 Å for Mn–O and 1.38 Å for O–O. This geometry was optimized using the basis sets of LanL2DZ for Mn and 6-31G* for other atoms. Subsequently, all calculations were performed by using the 6-311+G* basis set for dioxygen. The unrestricted SCF calculation of $[Mn^{III}(P)(O_2)]^-$ with the total charge of -1, spin multiplicity of 5, and without any other constraints gave the electron spin configuration of **S5** in Fig. 1. Then, all geometrical parameters were fully optimized without any restrictions. From the configuration of **S5**, the initial guess of the unrestricted SCF calculation was formed by alternation of spin occupation to match with the spin configuration of **S3**, giving an SCF solution with antiferromagnetic spin coupling. Then, the geometry was optimized. The ferromagnetic spin coupling of **S4** was obtained by spin-flip of the antiferromagnetic spin coupling in the spin configuration of **S3**. The electron spin configuration of **S1** was obtained by slightly changing the optimized geometry of **S3** and by using the spin configuration of **S3** without changing the spin occupation. The frequency analyses were performed for optimized geometries of all electron spin configurations, **S1**, **S3**, **S4**, and **S5** with side-on forms. The states with spin configurations of **S3** and **S5** have single imaginary frequency; then, we performed the intrinsic reaction coordinate (IRC) calculations in order to find the minimum states connecting the transition states.[34,35]

Analyses by Spin Densities and Natural Orbitals. In most cases, it is important to identify the formal oxidation state of a metal in order to elucidate the electronic structure in its metal-complex system. One of methods to identify the formal oxidation state is spin density on the metal, which can be estimated by Mulliken spin population. For $(3d)^5$ configuration of Mn(II), spin density is given by 5, and it is 4 for $(3d)^4$ configuration of Mn(III). The additional tool is to examine the value of total spin angular momentum $\langle S^2 \rangle$, which gives 6 for **S1**, 12 for **S4**, and 6 for **S5**. For **S3**, in which two spins are antiferromagnetically coupled, the $\langle S^2 \rangle$ value becomes different from 6 of the pure spin state due to the spin contaminations from the higher spin state in the broken symmetry solution. However, in the real calculations of the metal complexes, the spin density on metal and angular momentum are, sometimes, deviated from the pure values because of charge and spin delocalizations and redistributions. Accordingly, it is not possible in many cases to identify the electronic structure and the oxidation state of a metal from only spin density and spin angular momentum.

As an additional method, the analysis of natural orbital that is estimated by diagonalizing the density matrix of the desired state is a strong tool to identify the electron spin configuration. The natural orbital for the open-shell system is generally presented as follows:

$$\rho(r, r') = \sum_i n_{-i}\phi_{-i}(r)\phi^*_{-i}(r') + \sum_i n_{+i}\phi_{+i}(r)\phi^*_{+i}(r') + \sum_{i=1}^{m} \phi_i(r)\phi^*_i(r'). \quad (1)$$

Here, $n_{\pm i}$ are occupation numbers of electrons in the natural orbitals $\phi_{\pm i}(r)$ with

$$n_{-i} + n_{+i} = 2, \quad n_{\pm i} \geq 0. \quad (2)$$

In the case of $n_{-i} \cong 2$ and $n_{+i} \cong 0$, $\phi_{-i}(r)$ is a doubly occupied orbital. In the case of $n_{-i} \cong n_{+i} \cong 1$, $\phi_{-i}(r)$ and $\phi_{+i}(r)$ are the broken symmetry solutions with antiferromagnetic coupling of two spins. $\phi_i(r)$ is a singly occupied orbital (SOMO), and m corresponds to the number of spins in the open-shell system. For example, m-values are given by four for **S1**, **S3**, and **S5**. Accordingly, $\phi_i(r)$ shows a radical orbital with up-spin. For **S5** spin configuration, three SOMOs correspond to three different 3d orbitals, and one SOMO to the π^* orbital of the dioxygen. If we did not have this picture of SOMOs for **S5**, the obtained SCF solution would present a different electronic structure from the **S5** spin configuration; even the spin density and $\langle S^2 \rangle$ value are reasonable.

Spin angular momentum $\langle S^2 \rangle$ can be represented by occupation numbers as follows:

$$\langle S^2 \rangle = \frac{m}{2}\left(\frac{m}{2} + 1\right) + \sum_{i(n_{+i} \neq 0)} n_{-i}n_{+i}, \quad (3)$$

showing that deviation of the $\langle S^2 \rangle$ value from the pure spin state depends on $n_{\pm i}$ values, which correspond to orbitals with antiferromagnetic coupling of spins. For **S3** spin configuration, the $\langle S^2 \rangle$ value is, therefore, expected to increase by unity from six of the pure spin state ($S = 2$) because of antiferromagnetic spin coupling ($n_{\pm i} \cong 1$). Accordingly, the $\langle S^2 \rangle$ value is increased one by one with increasing number of antiferromagnetically coupled spins.

Using these procedures, the electronic structures of $[Mn(P)(O_2)]^-$ are identified for the unrestricted SCF solutions obtained from initial guesses of **S1**, **S3**, **S4**, and **S5** electron spin configurations, as discussed in the following section.

Results and Discussion

Geometries and Energetics. We have obtained six stationary states for $[Mn(P)(O_2)]^-$: four side-on forms (**1**, **2ts**, **3**, and **4ts**) and two end-on forms (**2** and **4**), as shown in Fig. 2. Figure 2 also shows the selected bond distances and the coordinate system employed in this work. Summarized in Table 1 are the total and relative energies with and without zero point

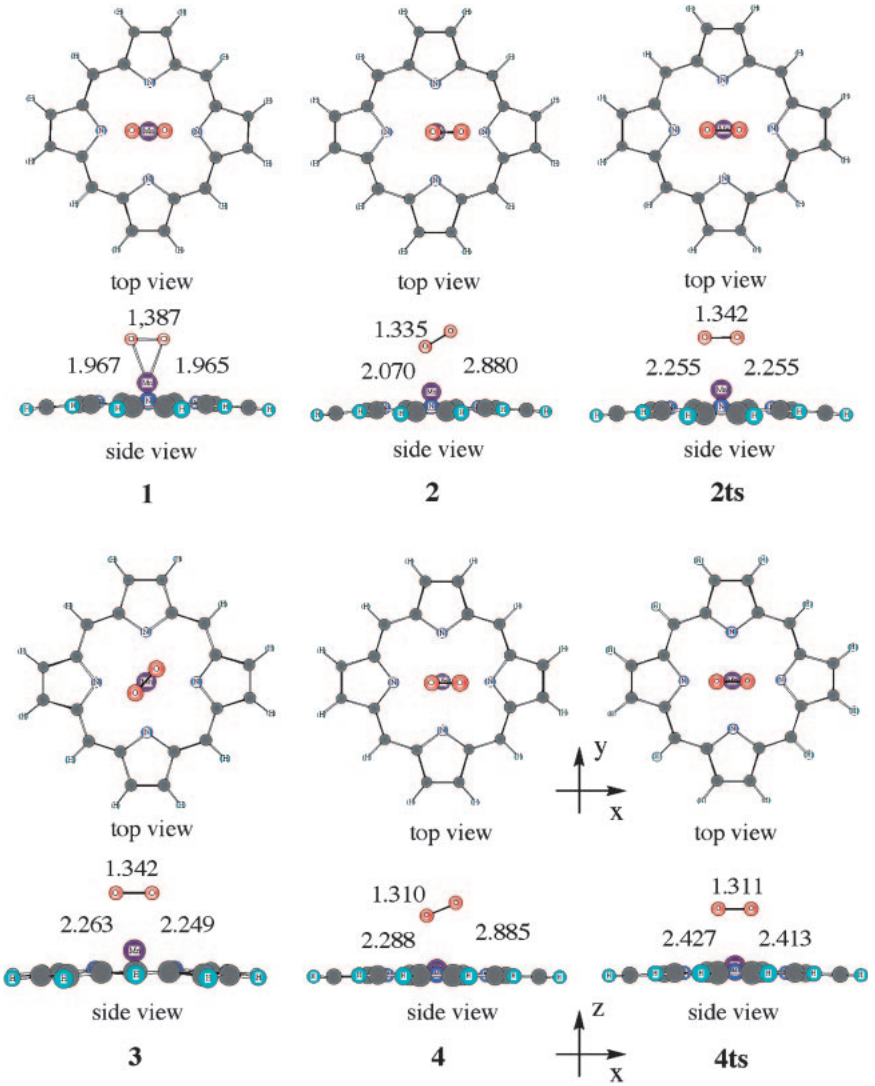

Fig. 2. Top and side views of optimized geometries of [Mn(P)(O$_2$)]$^-$. **1**, **2**, **3**, and **4** are local minimum states on the potential energy surface. **2ts** and **4ts** are transition states connecting to **2** and **4**, respectively. Distances are given in units of Å.

Table 1. Total Energies (au) and Relative Energies (kcal mol^{-1}) of Optimized Geometries of [Mn(P)(O$_2$)]$^-$ with and without Zero Point Corrections (ZPC)

State		Spin state	Without ZPC		With ZPC	
			$E_{total} + 1242$	ΔE_{rel}	$E_{total} + 1242$	ΔE_{rel}
1	$^5B_2$	Quintet	−0.824419	0.0	−0.548545	0.0
2	$^5A''$	Quintet	−0.824498	−0.0	−0.548868	−0.2
			(−0.825035	−0.4)[a)]		
2ts	$^5A_2$	Quintet	−0.822570	1.2	−0.547466	0.7
3	$^7A_2$	Septet	−0.824787	−0.2	−0.549456	−0.6
4	$^5A'$	Quintet	−0.795255	18.3	−0.518644	18.8
4ts	$^5A_1$	Quintet	−0.794293	18.9	−0.517923	19.2

a) Approximately projected energy estimated by Eq. 5 in text. The energy of the septet state is estimated by using the same geometry as the quintet state **2**. $^7E_U = -1242.821666$ au and $^7\langle S^2\rangle_U = 12.0109$.

corrections. From the frequency analyses, two side-on forms of **1** and **3** and two end-on forms of **2** and **4** are local minimum states on the potential energy surface with all positive frequencies, while two side-on forms of **2ts** and **4ts** are transition states with single imaginary frequencies of 100*i* and 88*i*, respectively. We performed the intrinsic reaction coordinate (IRC) calculations[34,35] from **2ts** and **4ts** in order to find the minimum states connecting to the transition states. **2ts** smoothly connects to

Table 2. Selected Bond Distances (Å) and Manganese Out-of-Plane Displacements (d_0) (Å) from Four Nitrogen Atoms in the Porphyrin Ring for Six Optimized Geometries of $[Mn(P)(O_2)]^-$ and the Observed Geometry

State	Mn–N(x)		Mn–N(y)		Mn–O		O–O	d_0/Å
1	2.203	2.206	2.224	2.224	1.965	1.967	1.387	0.795
2	2.190	2.191	2.185	2.185	2.070		1.335	0.712
2ts	2.209	2.209	2.191	2.191	2.255	2.255	1.342	0.673
3	2.198	2.198	2.198	2.200	2.249	2.263	1.342	0.709
4	2.048	2.051	2.052	2.053	2.288		1.310	0.255
4ts	2.057	2.058	2.054	2.054	2.413	2.427	1.311	0.218
$[Mn(TPP)(O_2)]^-$ [a]	2.151	2.184	2.199	2.202	1.888	1.901	1.421	0.764

a) Crystal structure of [peroxotetraphenylporphinato]manganate(III) given by Valentine et al.[8]

2, and **4ts** to **4**. **2ts** is only 0.9 kcal mol^{-1} higher in energy than **2**, and **4ts** is only 0.4 kcal mol^{-1} higher than **4**, as can be seen from Table 1, showing that dioxygen bound to Mn in **2** is easily shaken between **2** and **2ts**, and dioxygen in **4** is also easily shaken between **4** and **4ts**.

Table 2 lists the manganese–nitrogen, manganese–oxygen, and oxygen–oxygen distances and manganese out-of-plane displacements for six optimized geometries of $[Mn(P)(O_2)]^-$. In the side-on form of **1**, the Mn–O distances are 1.965 and 1.967 Å, and the O–O distance is 1.387 Å. These distances are in reasonable agreement with the 1.888 and 1.901 Å observed by the X-ray crystallographic study of $[Mn^{III}(TPP)(O_2)]^-$.[8] The Mn atom is 0.795 Å out of the plane of four nitrogen atoms in the porphyrin ring, which is also in reasonable agreement with the 0.764 Å of $[Mn^{III}(TPP)(O_2)]^-$. It could be, therefore, believed from these results that the side-on form **1** is expected to correspond to the observed side-on form of $[Mn^{III}(TPP)(O_2)]^-$, in harmony with **1** being a state optimized in geometry by the SCF solution converged with **S1** spin configuration as an initial guess.

From Table 1, **2** and **3** are isoenergetic to **1**, and only 0.2 and 0.6 kcal mol^{-1} different in energy, respectively. However, **2** has the end-on form, different from the side-on of **1**. The Mn–O distance is estimated to be 2.070 Å, longer than the 1.966 Å of **1**, while the O–O distance is 1.335 Å, shorter than the 1.387 Å of **1**. For the side-on form **3**, distances of Mn–O and O–O are 2.256 Å (in average of two Mn–O distances) and 1.342 Å, respectively, also being longer and shorter than those of **1**. However, the Mn atom is 0.712 and 0.709 Å out of the plane of four nitrogen atoms in the porphyrin ring for **2** and **3**, respectively, similar to the 0.795 Å of **1**.

The end-on form of **4** is higher in energy by 18.8 kcal mol^{-1} than **1**. The Mn–O distance is the longest and O–O distance is the shortest. Mn is only 0.255 Å out of the plane of four nitrogen atoms in the porphyrin ring, being essentially different from **1**, **2**, and **3**.

Electronic Structures. Four stable states, **1**, **2**, **3**, and **4**, were obtained based on the assumption of the electron spin configurations **S1**, **S3**, **S4**, and **S5**, respectively. It is, however, not clear whether the four stable states hold the original spin configurations or not. As can be seen from Fig. 1, spin configurations **S1**, **S3**, **S4**, and **S5** are easily distinguishable by spin densities on the Mn atom and dioxygen. For the **S1** spin configuration, the Mn atom has four up-spins and dioxygen has no spin due to fully occupied π^* orbitals. The Mn atom has five up-spins and dioxygen has a single down-spin for **S3**, while the Mn atom has five up-spins and dioxygen has a single up-spin for **S4**. For **S5**, the Mn atom has three up-spins and dioxygen has a single up-spin. Accordingly, the four spin configurations **S1**, **S3**, **S4**, and **S5** have essentially different patterns in spin distribution.

Table 3. Spin Angular Momentums ($\langle S^2 \rangle$) and Spin Densities of Mn, Porphyrin Ring (P), and Dioxygen (O–O) Moieties for Six Optimized Geometries of $[Mn(P)(O_2)]^-$

		Spin densities		
	$\langle S^2 \rangle$	Mn	P	O–O
1	6.4076	4.342	0.168	−0.510
2	6.9565	4.729	0.175	−0.905
2ts	6.9955	4.756	0.163	−0.919
3	12.0158	4.708	0.158	1.134
4	6.1500	2.900	−0.151	1.251
4ts	6.1503	2.885	−0.163	1.278

Summarized in Table 3 are spin angular momentums and spin densities of Mn, Porphyrin (P), and O–O moieties of four stable states and their transition states. Spin densities of P and O–O moieties were obtained by summation of the atomic spin densities in P and O–O moieties. As expected from the above considerations, it is easily found that the spin densities of $[Mn(P)(O_2)]^-$ are divided into four groups, (**1**), (**2** and **2ts**), (**3**), and (**4** and **4ts**). For **1**, spin angular momentum $\langle S^2 \rangle$ is 6.4076, slightly larger than the 6.0 of the pure quintet state with four parallel spins. Spin densities of Mn and O–O are estimated to be 4.324 and −0.510, respectively. It is expected from these results that **1** has four up-spins localized on Mn and small diradical character distributed on Mn and O–O with weak antiferromagnetic spin coupling. However, it seems that the pattern of spin densities of **1** holds that of **S1**: even Mn and O–O have extra spin densities.

The spin densities of Mn and O–O in **2** are 4.729 and −0.905, showing that Mn has five up-spins and O–O has a single down-spin. The $\langle S^2 \rangle$ value is 6.9565, which is increased by unity from the 6.0 of the pure quintet state. These results indicate that there exist spins with antiferromagnetic coupling between Mn and O–O, and an additional four up-spins on Mn; because of that the antiferromagnetic spin coupling increases $\langle S^2 \rangle$ by unity from the value of the pure spin state, as shown in above section.[36–38] Thus, the pattern of the spin densities of **2** holds that of **S3**. Spin densities of Mn and O–O in **3** are 4.708 and 1.134, respectively, showing that Mn has five up-spins and O–O has a single up-spin. The $\langle S^2 \rangle$ value is

Table 4. Occupation Numbers of Natural Orbitals of Optimized States of [Mn(P)(O$_2$)]$^-$, Characteristics of Natural Orbitals in Parenthesis, Diradical Characters, and Chemical Formula of Mn–O Bonds

Orbital	**1** (^{5}B$_2$)	**2** (^{5}A″)	**2ts** (^{5}A$_2$)	**3** (^{7}A$_2$)	**4** (^{5}A′)	**4ts** (^{5}A$_1$)
LUMO	0.226 ($d_{xz} - \pi_z^*$)			0.004 (P)	0.066 (P)	0.067 (P)
SOMO+1		0.771 ($d_{yz} - \pi_y^*$)	0.885 ($d_{xy} - \pi_y^*$)			
SOMO6				1.0 ($d_{x^2-y^2}$)		
SOMO5				1.0 (d_{xz})		
SOMO4	1.0 (d_{xy})	1.0 (d_{z^2})	1.0 (d_{xz})	1.0 (d_{yz})	1.0 (d_{z^2})	1.0 (π_y^*)
SOMO3	1.0 (d_{yz})	1.0 ($d_{x^2-y^2}$)	1.0 (d_{yz})	1.0 ($d_{xy} - \pi_y^*$)	1.0 (d_{xz})	1.0 (d_{xz})
SOMO2	1.0 (d_{z^2})	1.0 (d_{xy})	1.0 ($d_{x^2-y^2}$)	1.0 (d_{z^2})	1.0 (π_y^*)	1.0 (d_{z^2})
SOMO1	1.0 ($d_{x^2-y^2}$)	1.0 (d_{xz})	1.0 (d_{z^2})	1.0 ($d_{xy} + \pi_y^*$)	1.0 (d_{yz})	1.0 (d_{yz})
SOMO−1		1.229 ($d_{yz} + \pi_y^*$)	1.115 ($d_{xy} + \pi_y^*$)			
HOMO	1.774 ($\pi_z^* + d_{xz}$)	1.998 (π_y)	1.998 (π_y)	1.996 (π_z^*)	1.934 (π_z^*)	1.933 (π_z^*)
HOMO−1	1.998 (π_z)	2.000 (π_z^*)	1.999 (π_z^*)			
HOMO−2					1.998 (d_{xy})	
HOMO−4	2.000 (π_y^*)					1.998 (d_{xy})
b[a)]	0.032	0.565	0.773			
Formula	[Mn^{III}(O$_2^{2-}$)]$^-$		[Mn^{II}•(O$_2^{•-}$)]$^-$	[Mn^{II}•(O$_2^{•-}$)]$^-$	[Mn^{II}(O$_2^-$)]$^-$	

a) Diradical character estimated by Eq. 4 in text.

12.0158, which is nearly equal to the 12.0 of the septet state. Thus, the pattern of the spin densities of **3** holds that of **S4** with ferromagnetic spin coupling. The spin densities of Mn and O–O in **4** are 2.900 and 1.251, respectively, showing that Mn has three up-spins and O–O has a single up-spin, while the $\langle S^2 \rangle$ value of **4** is 6.1500, nearly equal to the 6.0 of the pure quintet state. **4** also holds the pattern of spin densities of **S5**. It is, therefore, confirmed that the four stable states **1**, **2**, **3**, and **4**, optimized in geometry based on the assumption of the electron spin configurations **S1**, **S3**, **S4**, and **S5**, hold the original spin configurations.

As can be seen from Fig. 1, the electron spin configurations **S1**, **S3**, **S4**, and **S5** do not include the information of orbitals and their interactions at all. For **S1** (**1**), although π_y^* and π_z^* orbitals (in coordinate system shown in Fig. 2) of O$_2^{2-}$ are doubly occupied, it is uncertain which of the 3d orbitals on Mn is unoccupied, and the orbital interactions between Mn and O$_2^{2-}$ are also unknown. For **S3** (**2**) and **S4** (**3**), it cannot be seen from Fig. 1 what 3d orbitals on Mn and π^* orbitals on O$_2^-$ contribute to the antiferromagnetic or ferromagnetic spin couplings. In the side-on form, the π_y^* orbital will interact with the d_{xy} orbital and π_z^* with d_{xz} due to the symmetry consideration. In the end-on form, the π_y^* orbital will interact with the d_{yz} orbital and π_z^* with d_{z^2} from symmetry consideration. For **S5** (**4**), it is uncertain which of the 3d orbitals on Mn is doubly occupied or unoccupied. It is apparent that these unknown electron configurations of [Mn(P)(O$_2$)]$^-$ are largely dependent on the geometric configuration of [Mn(P)(O$_2$)]$^-$.

In order to explore the electronic structures of **1**, **2**, **3**, and **4**, we performed the natural orbital (NO) analysis. Summarized in Table 4 are their occupation numbers and the orbital assignments in parentheses. The notation of SOMOi ($i = 1$–6) is used for the singly occupied NO with an occupation number of pure unity, indicating the pure radical orbital, as shown in Eq. 1. SOMO$-i$ is used for NOs with the occupation numbers (n_{-i}) greater than and nearly equal to unity, and HOMO and HOMO$-i$ are used with n_{-i} nearly equal to two. The corresponding NO with the occupation number n_{+i} ($n_{-i} + n_{+i} = 2$ in Eq. 2) is denoted by SOMO+i, LUMO, and LUMO+i. The diradical character b of NO can be estimated from the occupation number of n_- or n_+ as follows:[36–38]

$$b = 1 - \frac{2(n_- - 1)}{(n_- - 1)^2 + 1} = 1 - \frac{2(1 - n_+)}{(1 - n_+)^2 + 1}. \qquad (4)$$

It can be seen for **1** from Table 4 that four pure radicals with up-spins are localized on Mn and that the d^4 configuration is $(d_{xy})^1(d_{yz})^1(d_{x^2-y^2})^1(d_{z^2})^1$. This is in good agreement with $(d_{xy} - O_2\pi_{gy})^1(d_{yz})^1(d_{z^2})^1(d_{x^2-y^2})^1$ obtained from the previous IEH calculations[8] except for a small discrepancy. The IEH calculations yield that one of the singly occupied orbitals is given by the hybrid 60% d_{xy}–40% O$_2$ π_y^* through a mix of Mn d_{xy} and O$_2$ π_y^*. However, our B3LYP calculations give a singly occupied Mn d_{xy} orbital (94% d_{xy}–3% π_y^* (O$_2$)–3% π (P)) and doubly occupied O$_2$ π_y^* orbital, as can be seen from Fig. 3. The π_z^* orbital of dioxygen interacts with the d_{xz} orbital of Mn, yielding a strong bonding HOMO with the occupation number of 1.774 and antibonding LUMO with 0.226, as shown in Fig. 3. The deviation from 2.0 to 1.774 in the occupation number causes the spin polarization between Mn and dioxygen, reflecting the appearance of spin densities on Mn and dioxygen as shown in Table 3. It is, therefore, concluded that the electron configuration of **1** (^{5}B$_2$) obtained here strongly supports the suggestion by Valentine and co-workers,[8] and the oxidation state of Mn in **1** is Mn(III) rather than Mn(II). In addition, these results lead to the conclusion that the chemical formula of **1** (^{5}B$_2$) can be formally represented as [Mn^{III}(P)(O$_2^{2-}$)]$^-$.

Before the electronic structure of the minimum stationary state **2** is explored, it is interesting to elucidate it for the transition state **2ts**, which connects smoothly to **2**. **2ts** also has the same side-on form of dioxygen as the local minimum state **1**. It is easily found from Table 4 that four pure radicals are localized on Mn with a d^4 configuration of $(d_{xz})^1(d_{yz})^1(d_{x^2-y^2})^1(d_{z^2})^1$. The d_{xz} orbital of this configuration is different from the d_{xy} orbital of $(d_{xy})^1(d_{yz})^1(d_{x^2-y^2})^1(d_{z^2})^1$ for **1**. The π_y^* orbital is destabilized with shorting the O–O distance from 1.387 to

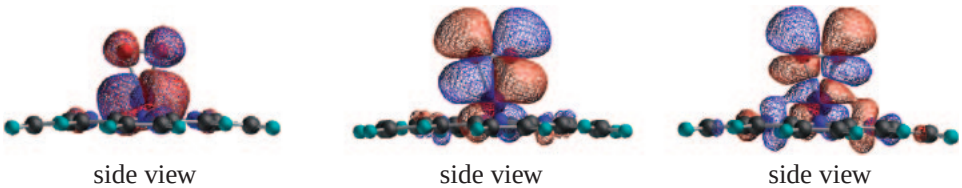

Fig. 3. Side views of SOMO4, HOMO, and LUMO for side-on form **1**.

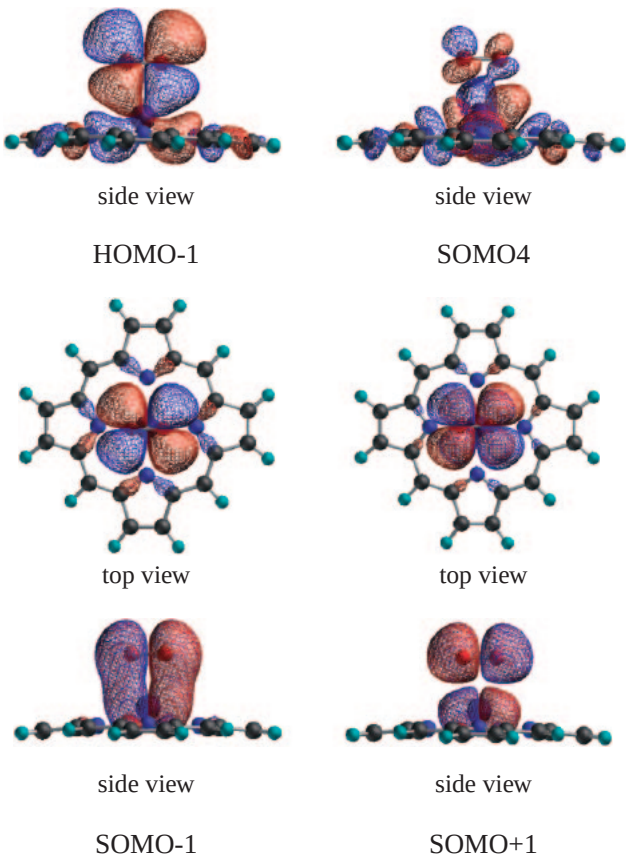

Fig. 4. Side views of HOMO−1 and SOMO4 and top and side views of SOMO−1 and SOMO+1 for the side-on form **2ts**.

1.342 Å, as shown in Table 2, yielding bonding and antibonding interactions with d_{xy} that have occupation numbers of 1.115 and 0.885, respectively. These orbitals are shown as SOMO−1 and SOMO+1 in Fig. 4. The diradical character b of these orbitals can be estimated using Eq. 4. The diradical character is 0.773, showing that the antiferromagnetically coupled spins are distributed on d_{xy} of Mn and π_y^* of O–O. These are consistent with the spin densities of 4.756 on Mn and −0.919 on O–O, and the $\langle S^2 \rangle$ value is increased by about unity from the pure spin state as shown by Eq. 3. The π_z^* orbital does not interact with d_{xz} due to the longer distance of 2.255 Å (1.966 Å for **1**), yielding that d_{xz} is changed to a pure radical orbital and π_z^* is changed to a doubly occupied orbital, as shown in Fig. 4. They are different from the mixing of d_{xz} and π_z^* in the side-on form of **1**. Since Mn has four pure radical spins and a single diradical spin coupled with O–O, the oxidation state of Mn is Mn(II) rather than Mn(III). It is, therefore, concluded that **2ts** ($^5A_2$) is characterized by $[Mn^{II\bullet}(P)(O_2^{\bullet -})]^-$ as a formal chemical formula.

Geometric change from **2ts** to **2** induces reduction of symmetry from C_{2v} to C_s. d_{xy} and d_{yz} orbitals in **2ts**, which have respectively a_2 and b_1 symmetries of C_{2v}, belong to the same symmetry a'' in C_s of **2**. In the end-on form of **2**, one of the dioxygens is 2.070 Å from Mn and the other is 2.880 Å away from Mn. Accordingly, the π_y^* orbital interacts with the d_{yz} orbital rather than d_{xy}, and d_{xy} is switched to the pure radical orbital in place of the d_{yz} of **2ts**. SOMO−1 and SOMO+1, which correspond to diradical orbitals with antiferromagnetic spin coupling, are depicted in Fig. 5. It is easily found that SOMO−1 is the bonding interaction of d_{yz} and π_y^*, and SOMO+1 is the antibonding interaction. These indicate that the electronic structure of **2** ($^5A''$) is smoothly connected to those of **2ts** ($^5A_2$).

As expected from the previous discussion that **3** (side-on form) holds the **S4** spin configuration, d_{xy} and π_y^* orbitals with the antiferromagnetic spin coupling in **2ts** are changed to diradical orbitals with the ferromagnetic spin coupling. **2** and **3** are isoenergetic with only 0.2 kcal mol^{-1} of difference without zero point correction (Table 1). The unrestricted solution for **2** with the antiferromagnetic spin coupling suffers from spin contamination from the next higher spin state. In this case, the septet spin state is the main contamination, which can be approximately removed. The total energy $^5E_{PU}$ after removal of spin contamination is obtained using the energies ^5E_U, energy of the unrestricted solution for the quintet state, and ^7E_U, energy for the septet state with the geometry of ^5E_U state, as follows:[36–38]

$$^5E_{PU} = {}^5E_U + \frac{{}^5\langle S^2\rangle_U - {}^5\langle S^2\rangle}{{}^7\langle S^2\rangle - {}^5\langle S^2\rangle_U}({}^5E_U - {}^7E_U). \quad (5)$$

The evaluated value is listed in parenthesis in Table 1. Although **2** and **3** are still isoenergetic, **2** is lower by 0.2 kcal mol^{-1} in relative energy than **3**. Shirazi and Goff provided a prediction from the observation of downfield NMR shifts for the pyrrole protons that Mn is a high-spin state with a singly occupied $d_{x^2-y^2}$ orbital and is Mn(II) rather than Mn(III).[10] They also proposed that the Mn(II) center has strong antiferromagnetic coupling to the unpaired spin on a superoxo ligand.[10] Their proposal is in good agreement with the electronic structure of **2** obtained here. **2** has a singly occupied $d_{x^2-y^2}$ and strong antiferromagnetic spin coupling between d_{yz} and π_y^*, as can be seen from Table 4 and Fig. 5. In other words, the geometry and electronic structure of **2** support strongly the observation by Shirazi and Goff rather than that by Valentine and co-workers.[8,11] The observations of two different electronic

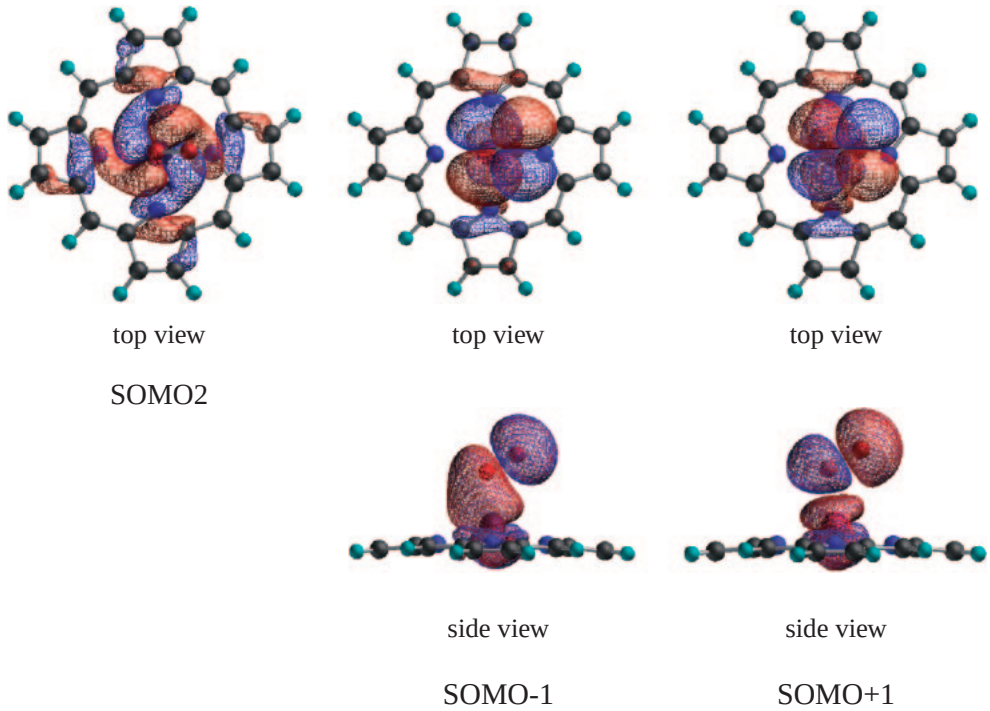

Fig. 5. Top view of SOMO2 and top and side views of SOMO−1 and SOMO+1 for the end-on form **2**.

structures and geometries of **1** (^{5}B$_2$) and **2** (^{5}A″) might be due to the difference of experimental conditions, where **1** is observed in a crystal and **2** in a Me$_2$SO solution. Unfortunately, we could not find the experimental observation corresponding to the electronic structure of **3** (^{7}A$_2$). It might be possible, however, to observe it under the appropriate condition because of being isoenergetic to **2**.

The ground states of [Fe^{II}(P)(O$_2$)], which is an isoelectronic system to [Mn^{III}(P)(O$_2$)]$^-$, have end-on forms.[39–43] The electronic structure is a singlet diradical state in which two spins are distributed on Fe and dioxygen with an antiferromagnetic coupling.[39–43] The diradical orbitals are presented by bonding and antibonding interactions of d_{yz} and π_y*, being essentially similar to antiferromagnetic coupling of spins in **2**. The difference between [Fe^{II}(P)(O$_2$)] and **2** is that Fe has no pure radical spins from d orbitals due to double occupation of electrons, and Mn has four pure radical spins from d orbitals such as $(d_{xy})^1(d_{xz})^1(d_{x^2-y^2})^1(d_{z^2})^1$ shown in Table 4. It is interesting that end-on forms of dioxygen to Mn and Fe give the same antiferromagnetic spin coupling in spite of showing different behaviors of Mn and Fe in the chemical and biological systems.

4 is 19 kcal mol^{-1} higher in relative energy than **1**, **2**, and **3**, and the geometry of **4** is quite different from those of **1**, **2**, and **3** (see Fig. 2). The out-of-plane distance of Mn for four nitrogen atoms in the porphyrin ring is only 0.255 Å, remarkably shorter than the 0.795, 0.712, and 0.709 Å of **1**, **2**, and **3**, respectively, as shown in Table 2. Mn is, thus, closer to four nitrogen atoms, when compared with **1**, **2**, and **3**, reflecting the shortest Mn–N distances among **1**, **2**, **3**, and **4**. Figure 6 shows the contour maps of HOMO−2, SOMO1, and SOMO2. HOMO−2 is composed of $d_{x^2-y^2}$ and π_y of O–O (66% $d_{x^2-y^2}$ + 24% π_y (O–O) − 10% σ* (P)), while two SOMOs are composed of d_{yz} and π_y* of O–O. The π_y* is made more unstable with shortening the O–O distance to 1.310 Å. The long Mn–O distance causes loss of interaction between π_y* and d_{yz}, resulting in π_y* and d_{yz} being shifted to pure radical orbitals with the occupation number of unity. $d_{x^2-y^2}$ which appears as a pure radical orbital for **1** and **2**, is shifted to the unoccupied orbital because of strong antibonding interaction with four nitrogen atoms in the porphyrin ring due to the small out-of-plane distance. For the **S5** (**4**) spin configuration shown in Fig. 1, the doubly occupied orbital in Mn is d_{xy}, the unoccupied orbital in Mn is $d_{x^2-y^2}$, and the singly occupied orbital in dioxygen is π_y*. Therefore, the electron configuration of Mn for **4** is given by $(d_{xy})^2(d_{z^2})^1(d_{xz})^1(d_{yz})^1$, showing that the oxidation state of Mn is Mn(II). Unfortunately, we could not find any experimental observation corresponding to the electronic structure of **4**. Finally, the chemical formula of **4** (^{5}A′) is formally represented as [Mn^{II}(P)(O$_2^{\bullet-}$)]$^-$.

Summary

Geometries and electronic structures of [Mn(P)(O$_2$)]$^-$ have been investigated in this work. We have explored all stable states corresponding to the possible electron spin configurations. In the addition of O$_2^-$ to Mn–porphyrin, four geometries, **1** (^{5}B$_2$), **2** (^{5}A″), **3** (^{7}A$_2$), and **4** (^{5}A′) with essentially different electronic structures were found. **1** and **3** have side-on forms and **2** and **4** have end-on forms. We clarified from our theoretical views that the two states **1** and **2** with perfectly different electron configurations are discussed on the same stage of the experiment. Our results are summarized as follows:

1) For the side-on form **1** (^{5}B$_2$), the electron configuration of [Mn(P)(O$_2$)]$^-$ is presented by $(\pi_y^*)^2(\pi_z^* + d_{xz})^2(d_{xy})^1(d_{yz})^1(d_{z^2})^1(d_{x^2-y^2})^1$. d_{xz} and π_z* provide the strong bonding orbitals and four pure radical spins are from 3d orbitals of

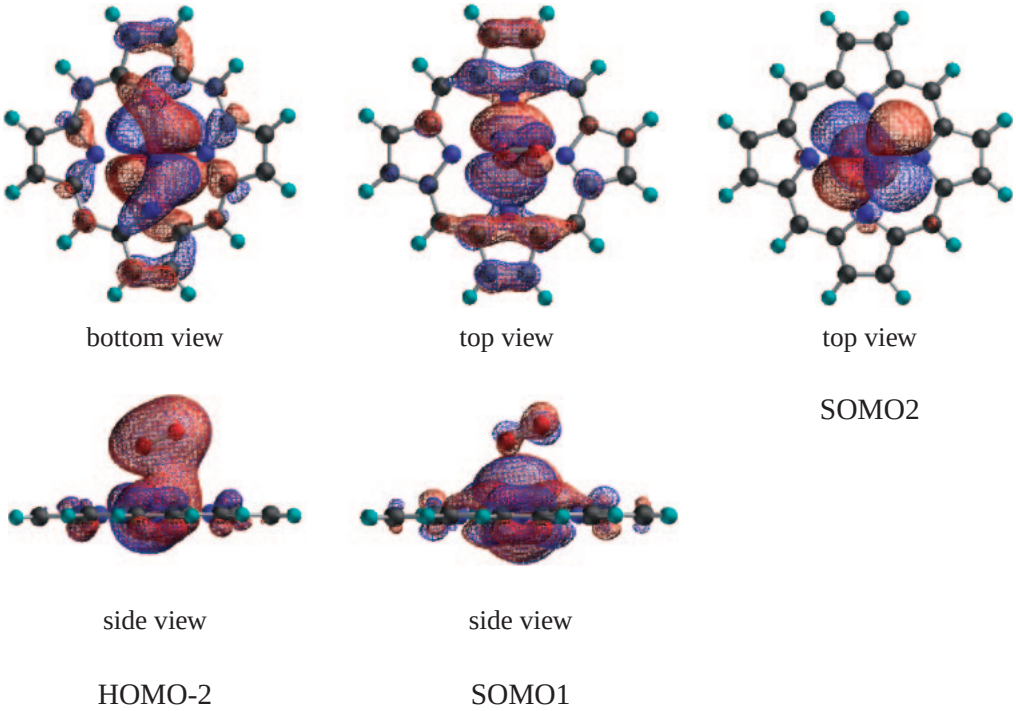

Fig. 6. Bottom and side views of HOMO−2, top and side views of SOMO1, and top view of SOMO2 for the end-on form **4**.

Mn. Formal presentation of the bond character in **1** is $[Mn^{III}(P)(O_2^{2-})]^-$. The side-on form **1** supports strongly the structure observed by X-ray crystallographic analysis.[8,11] The manganese atom is 0.795 Å out of the plane of four nitrogen atoms in the porphyrin ring, in good agreement with the 0.762 Å of the X-ray structure.

2) For the end-on form **2** ($^5A''$), d_{yz} and π_y^* provide antiferromagnetically coupled diradical spins with the electron configuration of $(\pi_z^*)^2(d_{xy})^1(d_{yz})^1(d_{xz})^1(d_{z^2})^1(d_{x^2-y^2})^1(\pi_y^*)^1$. Formal presentation of the bond character for **2** is $[Mn^{II\bullet}(P)(O_2^{\bullet-})]^-$. The end-on form **2** supports strongly the observation by Shirazi and Goff.[10] The $d_{x^2-y^2}$ orbital of Mn is singly occupied, and the d_{yz} orbital of Mn and π_y^* orbital have the strong antiferromagnetic coupling, yielding diradical character between Mn and dioxygen.

3) For the side-on form **3** ($^7A_2$), the electron configuration is given by $(\pi_z^*)^2(d_{xy})^1(d_{yz})^1(d_{xz})^1(d_{z^2})^1(d_{x^2-y^2})^1(\pi_y^*)^1$ with ferromagnetically coupled spins of d_{yz} and π_y^*. The ground state of **3** is a septet state, different from the quintet state of **2**. Formal presentation of the bond character for **3** is $[Mn^{II\bullet}(P)(O_2^{\bullet-})]^-$.

4) For the end-on form **4** ($^5A'$), four pure radicals are composed of π_y^* of O–O and three 3d of Mn with the electron configuration of $(\pi_z^*)^2(d_{xy})^2(d_{yz})^1(d_{xz})^1(d_{z^2})^1(\pi_y^*)^1$. Formal presentation of the bond character in **4** is $[Mn^{II}(P)(O_2^-)]^-$. The end-on form **4** is 19 kcal mol^{-1} higher in energy than **1**, **2**, and **3**.

This study has sparked our interest to investigate the potential energy surfaces from the stable states to the dissociation limits. We plan to perform them as a future study.

This work was supported by The Japanese Ministry of Education, Culture, Sports, Science and Technology.

References

1 V. L. Pecoraro, M. J. Baldwin, A. Gelasco, *Chem. Rev.* **1994**, *94*, 807.
2 B. B. Keele, Jr., J. M. McCord, I. Fridovich, *J. Biol. Chem.* **1970**, *245*, 6176.
3 A. Willing, H. Follmann, G. Auling, *Eur. J. Biochem.* **1988**, *170*, 603.
4 A. Willing, H. Follmann, G. Auling, *Eur. J. Biochem.* **1988**, *175*, 167.
5 K. N. Ferreira, T. M. Iverson, K. Maghlaoui, J. Barber, S. Iwata, *Science* **2004**, *303*, 1831.
6 C. Bull, R. G. Fisher, B. M. Hoffman, *Biochem. Biophys. Res. Commun.* **1974**, *59*, 140.
7 C. J. Weschler, B. M. Hoffman, F. Basolo, *J. Am. Chem. Soc.* **1975**, *97*, 5278.
8 R. B. VanAtta, C. E. Strouse, L. K. Hanson, J. S. Valentine, *J. Am. Chem. Soc.* **1987**, *109*, 1425.
9 J. S. Valentine, A. E. Quinn, *Inorg. Chem.* **1976**, *15*, 1997.
10 A. Shirazi, H. M. Goff, *J. Am. Chem. Soc.* **1982**, *104*, 6318.
11 M. F. Sisemore, M. Selke, J. N. Burstyn, J. S. Valentine, *Inorg. Chem.* **1997**, *36*, 979.
12 R. Zwaans, J. H. van Lenthe, D. H. W. den Boer, *THEOCHEM* **1995**, *339*, 153.
13 R. Zwaans, J. H. van Lenthe, D. H. W. den Boer, *THEOCHEM* **1995**, *367*, 15.
14 F. G. Doro, J. R. L. Smith, A. G. Ferreira, M. D. Assis, *J. Mol. Catal. A: Chem.* **2000**, *164*, 97.
15 D. A. Plattner, D. Feichtinger, J. El-Bahraoui, O. Wiest, *Int. J. Mass Spectrom.* **2000**, *195/196*, 351.
16 D. Rutkowska-Zbik, M. Witko, E. M. Serwicka, *Catal. Today* **2004**, *91–92*, 137.
17 M. J. de Groot, R. W. A. Havenith, H. M. Vinkers, R. Zwaans, N. P. E. Vermeulen, J. H. van Lenthe, *J. Comput.-Aided*

Mol. Des. **1998**, *12*, 183.
18 J. T. Groves, M. K. Stern, *J. Am. Chem. Soc.* **1987**, *109*, 3812.
19 J. T. Groves, M. K. Stern, *J. Am. Chem. Soc.* **1988**, *110*, 8628.
20 J. T. Groves, J. Lee, S. S. Marla, *J. Am. Chem. Soc.* **1997**, *119*, 6269.
21 A. D. Becke, *J. Chem. Phys.* **1993**, *98*, 1372.
22 A. D. Becke, *J. Chem. Phys.* **1993**, *98*, 5648.
23 A. D. Becke, *Phys. Rev. A* **1998**, *38*, 3098.
24 P. J. Stevens, F. J. Devlin, C. F. Chablowski, M. J. Frish, *J. Phys. Chem.* **1994**, *98*, 11623.
25 H. Tatewaki, S. Huzinaga, *J. Chem. Phys.* **1979**, *71*, 4339.
26 Y. Takahara, K. Yamaguchi, T. Fueno, *Chem. Phys. Lett.* **1989**, *158*, 95.
27 A. J. H. Wachters, *J. Chem. Phys.* **1970**, *52*, 1033.
28 M. A. Vincent, Y. Yoshioka, H. F. Schaefer, III, *J. Phys. Chem.* **1982**, *88*, 3905.
29 P. B. Armentrout, L. F. Halle, J. L. Beauchamp, *J. Am. Chem. Soc.* **1981**, *103*, 6501.
30 P. J. Hay, W. R. Wadt, *J. Chem. Phys.* **1985**, *82*, 270.
31 P. C. Hariharan, J. A. Pople, *Theor. Chim. Acta* **1973**, *28*, 213.
32 A. D. McLean, G. S. Chandler, *J. Chem. Phys.* **1980**, *72*, 5639.
33 M. J. Frisch, G. W. Trucks, H. B. Schlegel, G. E. Scuseria, M. A. Robb, J. R. Cheeseman, V. G. Zakrzewski, J. A. Montgomery, Jr., R. E. Stratmann, J. C. Burant, S. Dapprich, J. M. Millam, A. D. Daniels, K. N. Kudin, M. C. Strain, O. Farkas, J. Tomasi, V. Barone, M. Cossi, R. Cammi, B. Mennucci, C. Pomelli, C. Adamo, S. Clifford, J. Ochterski, G. A. Petersson, P. Y. Ayala, Q. Cui, K. Morokuma, D. K. Malick, A. D. Rabuck, K. Raghavachari, J. B. Foresman, J. Cioslowski, J. V. Ortiz, B. B. Stefanov, G. Liu, A. Liashenko, P. Piskorz, I. Komaromi, R. Gomperts, R. L. Martin, D. J. Fox, T. Keith, M. A. Al-Laham, C. Y. Peng, A. Nanayakkara, C. Gonzalez, M. Challacombe, P. M. W. Gill, B. Johnson, W. Chen, M. W. Wong, J. L. Andres, C. Gonzalez, M. Head-Gordon, E. S. Replogle, J. A. Pople, *Gaussian 98, Revision A.6*, Gaussian, Inc., Pittsburgh PA, **1998**.
34 C. Gonzalez, H. B. Schlegel, *J. Chem. Phys.* **1989**, *90*, 2154.
35 C. Gonzalez, H. B. Schlegel, *J. Chem. Phys.* **1990**, *94*, 5523.
36 Y. Yoshioka, D. Yamaki, G. Maruta, T. Tsunesada, K. Takada, T. Noro, K. Yamaguchi, *Bull. Chem. Soc. Jpn.* **1996**, *69*, 3395.
37 M. Nishino, S. Yamanaka, Y. Yoshioka, K. Yamaguchi, *J. Phys. Chem.* **1997**, *101*, 705.
38 Y. Yoshioka, D. Yamaki, S. Kiribayashi, T. Tsunesada, M. Nishino, K. Yamaguchi, K. Mizuno, I. Saito, *Electron. J. Theor. Chem.* **1977**, *2*, 218.
39 C. Rovira, P. Ballone, M. Parrinello, *Chem. Phys. Lett.* **1997**, *271*, 247.
40 C. Rovira, K. Kunc, J. Hutter, P. Ballone, M. Parrinello, *Int. J. Quantum Chem.* **1998**, *69*, 31.
41 C. Rovira, K. Kunc, J. Hutter, P. Ballone, M. Parrinello, *J. Phys. Chem. A* **1997**, *101*, 8914.
42 Y. Yoshioka, H. Kawai, K. Yamaguchi, *Chem. Phys. Lett.* **2003**, *374*, 45.
43 Y. Yoshioka, M. Mitani, *Internet Electron. J. Mol. Des.* **2003**, *2*, 732.